Supplementary Information for

KTlO: A metal shrouded 2D semiconductor with high carrier mobility and tunable magnetism

Ya-Qian Song,[1+] Jun-Hui Yuan,[1+] Li-Heng Li,[1] Ming Xu,[1] Jia-Fu Wang,[2] Kan-Hao Xue,[1,3*] and Xiang-Shui Miao[1]

[1] Wuhan National Research Center for Optoelectronics, School of Optical and Electronic Information, Huazhong University of Science and Technology, Wuhan 430074, China

[2] School of Science, Wuhan University of Technology, Wuhan 430070, China

[3] IMEP-LAHC, Grenoble INP – Minatec, 3 Parvis Louis Néel, 38016 Grenoble Cedex 1, France

[+]The authors Y.-Q. Song and J.-H. Yuan contributed equally to this work.

Corresponding Author

*E-mail: xkh@hust.edu.cn (K.-H. Xue)

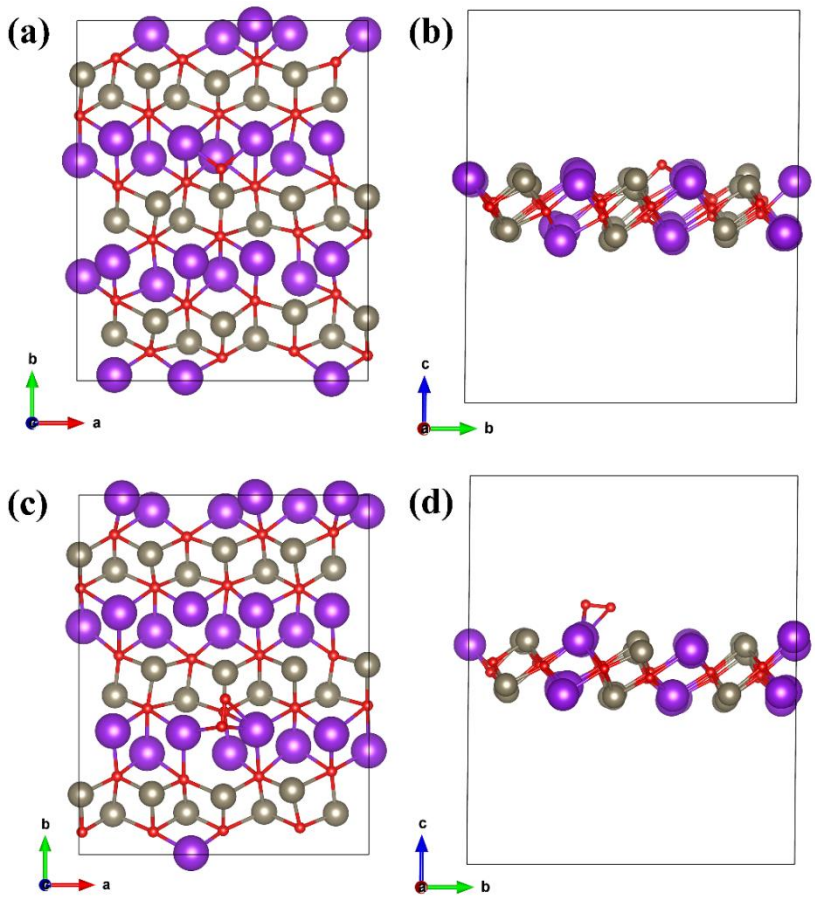

Figure S1. *Ab initio* molecular dynamics (AIMD) simulation for a single O atom/O_2 molecule on monolayer KTlO at 300K. (a) Top and (b) side view of an isolated O atom on monolayer KTlO during the simulation time of 10 ps at 300 K; (c) top and (d) side view of an isolated O_2 molecule on monolayer KTlO during the simulation time of 10 ps at 300 K.

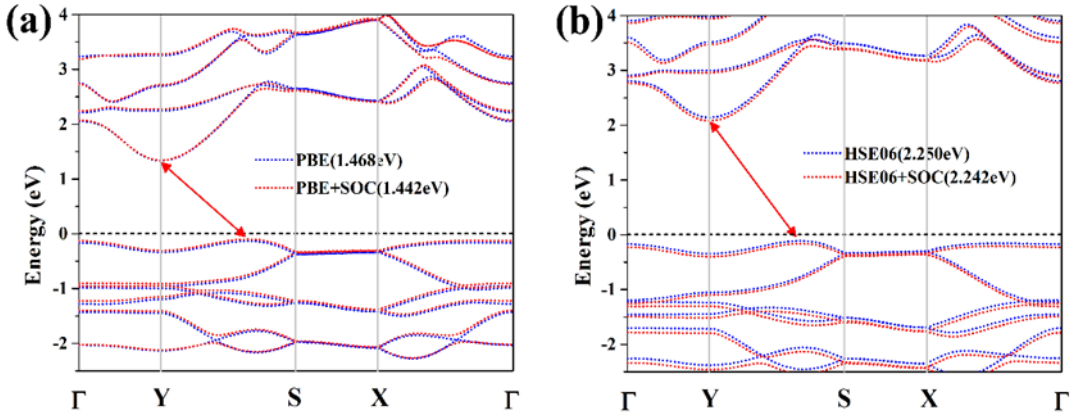

Figure S2. (a) Electronic band structures of monolayer KTlO at the PBE level, with or without considering spin-orbit coupling. (b) Electronic band structures of monolayer KTlO calculated using the screened HSE06 hybrid functional, with or without considering spin-orbit coupling.

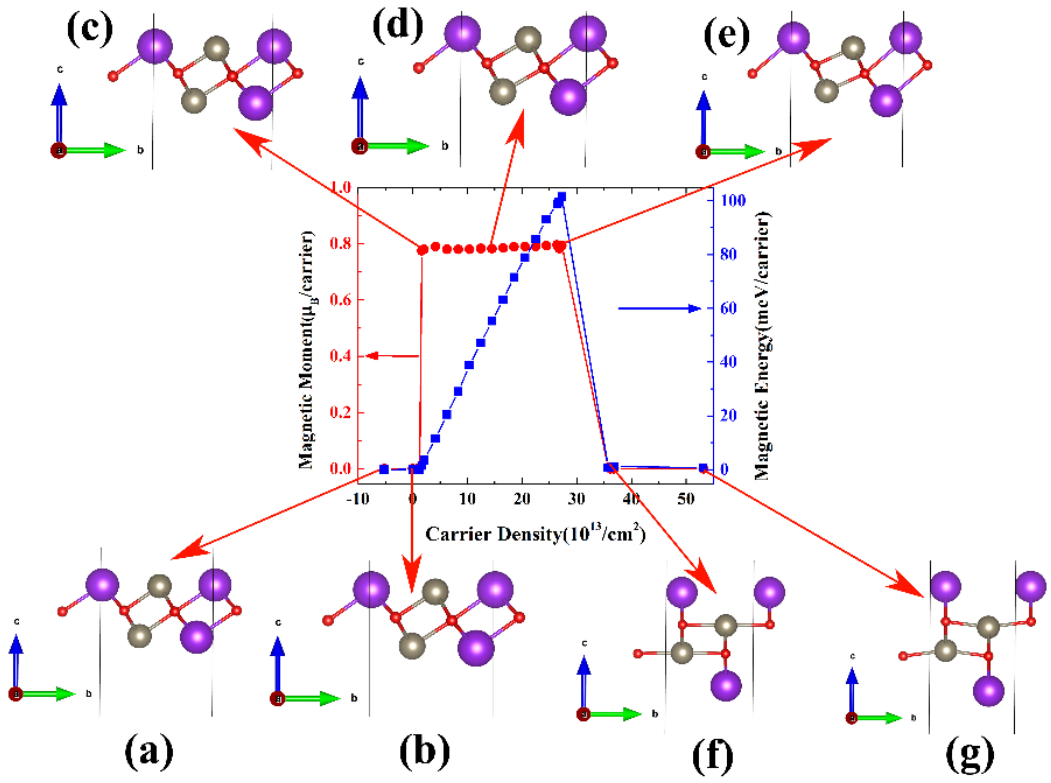

Figure S3. Optimized crystal structures of monolayer KTlO versus various electron/hole-doping levels: (a) -5.2×10^{13} cm^{-2}; (b) 0; (c) 1.67×10^{13} cm^{-2}; (d) 16.54 ×10^{13} cm^{-2}; (e) 27.3×10^{13} cm^{-2}; (f) 35.7×10^{13} cm^{-2}; (g) 53.2×10^{13} cm^{-2}. Positive and negative values stand for electron doping and hole doping, respectively.

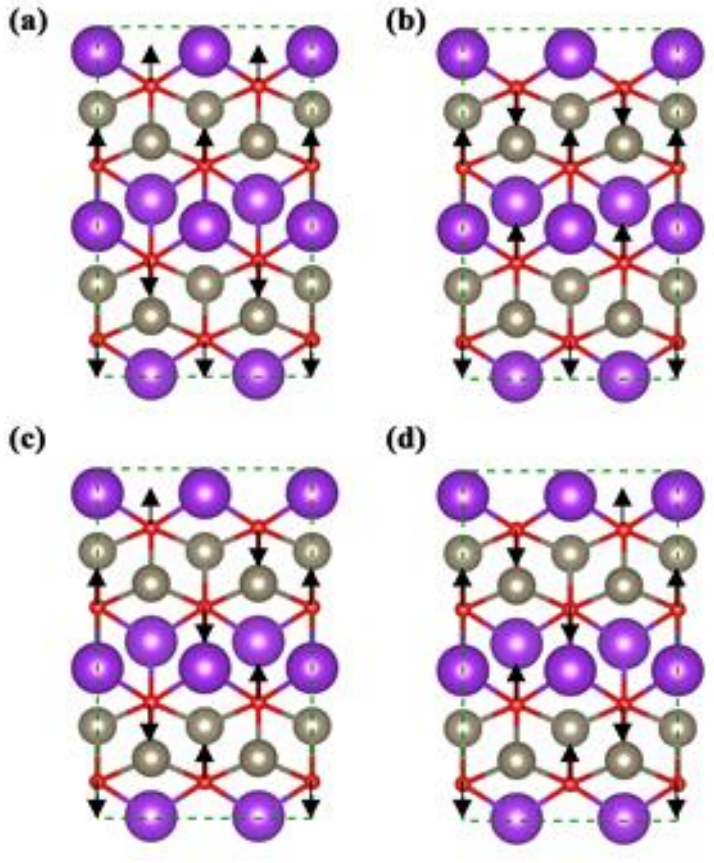

Figure S4. Various anti-ferromagnetic configurations with orientated up (↑) and down (↓) spins on oxygen atoms being considered in this work. The magnetic moments of potassium and thallium atoms are set to zero as the magnetic properties are dominated by the oxygen atoms.

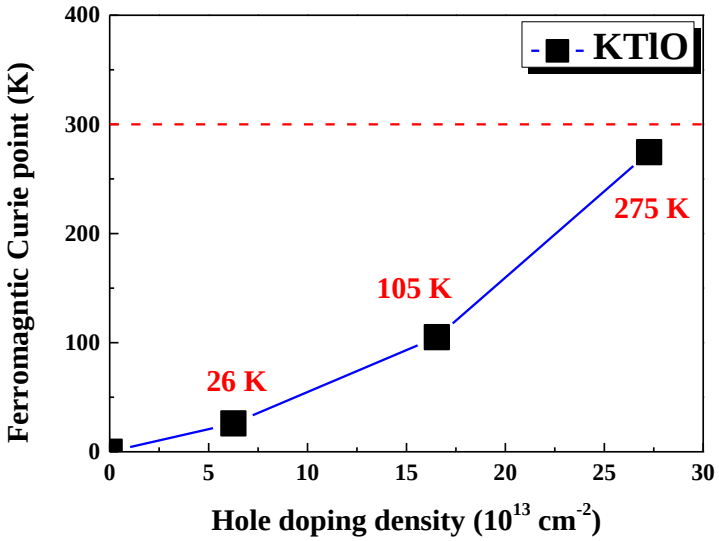

Figure S5. The hole doping concentration-dependent FM Curie temperatures in KTlO monolayer.

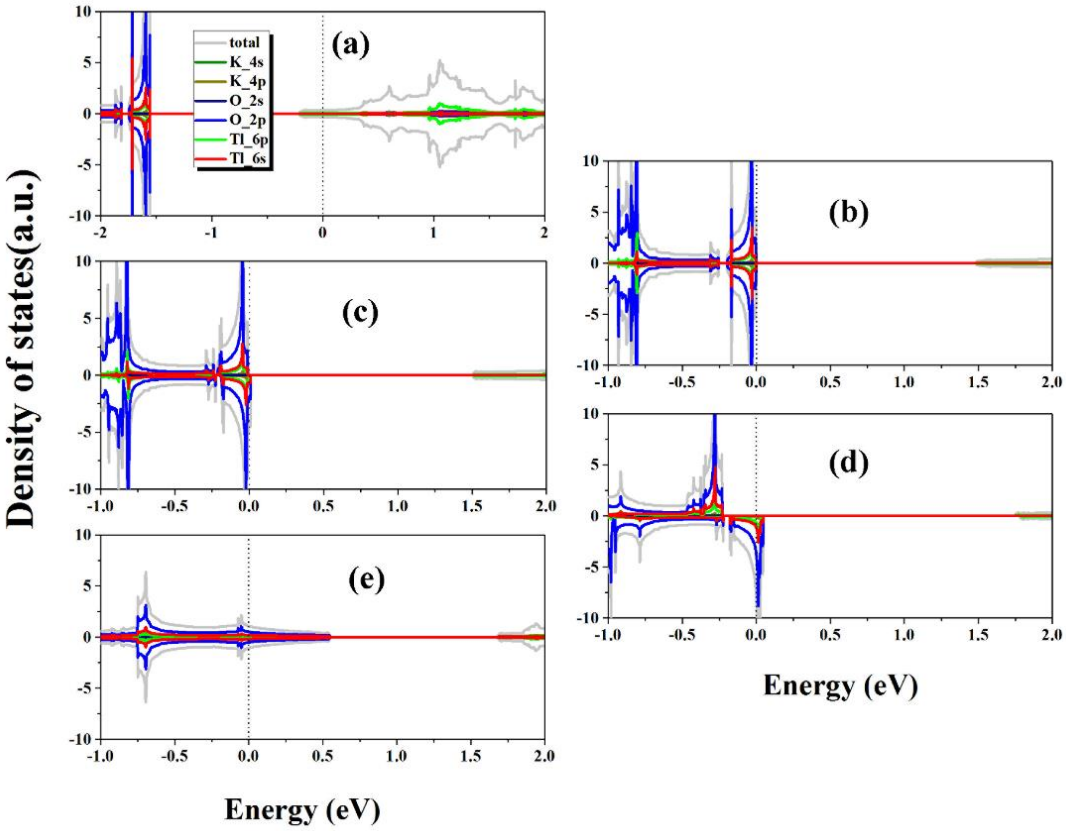

Figure S6. Projected density of states of monolayer KTlO versus various electron/hole-doping levels: (a) -5.2×10^{13} cm^{-2}; (b) 0; (c) 1.67×10^{13} cm^{-2}; (d) 16.54×10^{13} cm^{-2}; (e) 36.83×10^{13} cm^{-2}. Positive and negative values stand for electron doping and hole doping, respectively.

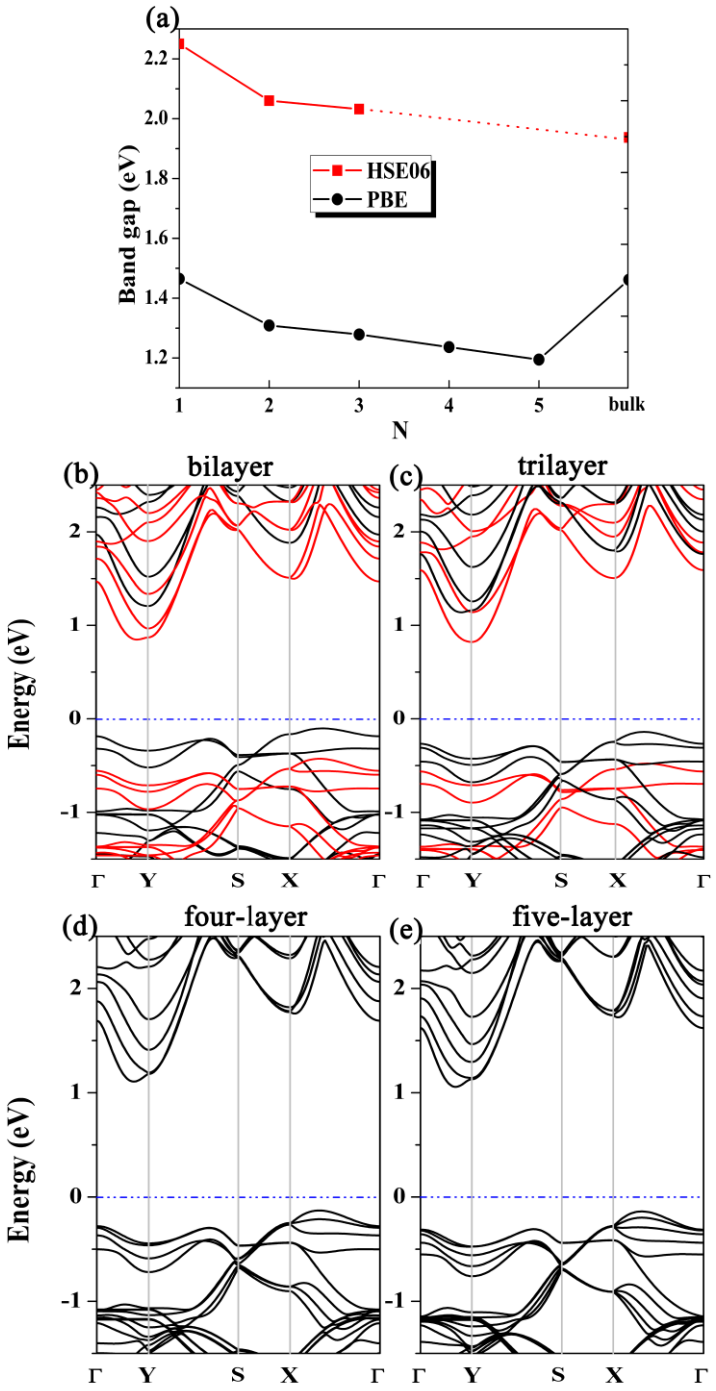

Figure S7. Electronic band structures of KTlO multilayers. (a) Computed band gaps of KTlO multilayers versus the number of atomic layers, using GGA-PBE and HSE06 functionals, respectively. Electronic band diagrams of (b) bilayer and (c) trilayer KTlO, calculated using the PBE functional (black line) and screened HSE06 hybrid functional (red line), respectively. Electronic band diagrams of (d) four-layer and (e) five-layer KTlO, calculated using the PBE functional.

Table S1. The carrier mobility μ_{2D} ($\times 10^3$ cm^2 V^{-1}s^{-1}) and energy bang gap (eV) at the HSE06 level (*d*/*i* represent direct/indirect band gaps) of KTlO, together with the values for Tl_2O and K_2O for comparison.

	Direction	KTlO	Tl_2O[1]	K_2O[2]
electron	*x*	0.20	3.342	8.80
	y	2.54	0.404	18.7
hole	*x*	1.86	4.302	0.005
	y	0.04	0.016	0.0003
band gap		2.25 (*i*)	1.56 (*d*)	1.288 (*i*)

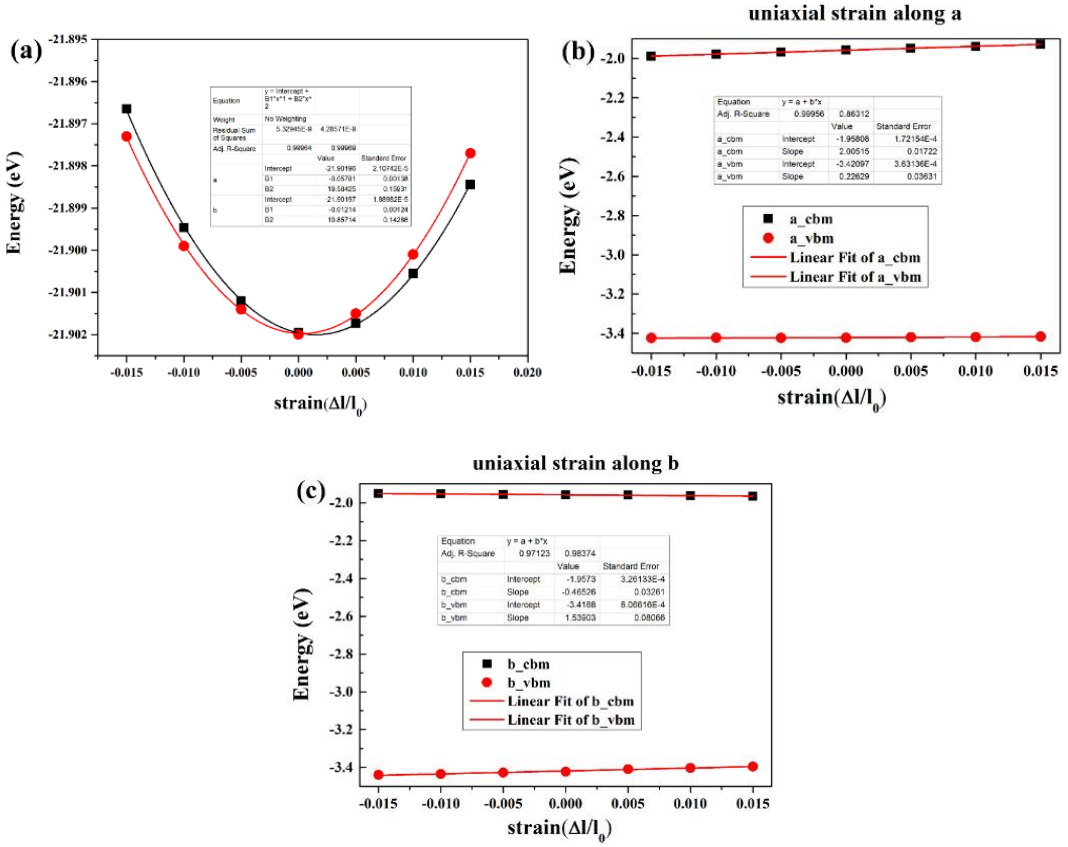

Figure S8. (a) Relation between the total energy and the applied strain δ along the *a* (black curve) and *b* (red curve) directions of monolayer KTlO. The quadratic fitting of the data gives the in-plane stiffness of 2D structures. (b) The VBM/CBM shifts for monolayer KTlO with respect to the vacuum energy, as a function of the applied strain along the *a* direction. (c) The VBM/CBM shifts for monolayer KTlO with respect to the vacuum energy, as a function of the applied strain along the *b* direction. The linear fit of the data in (b) and (c) gives the deformation potential constants. All the calculations were based on the PBE functional.

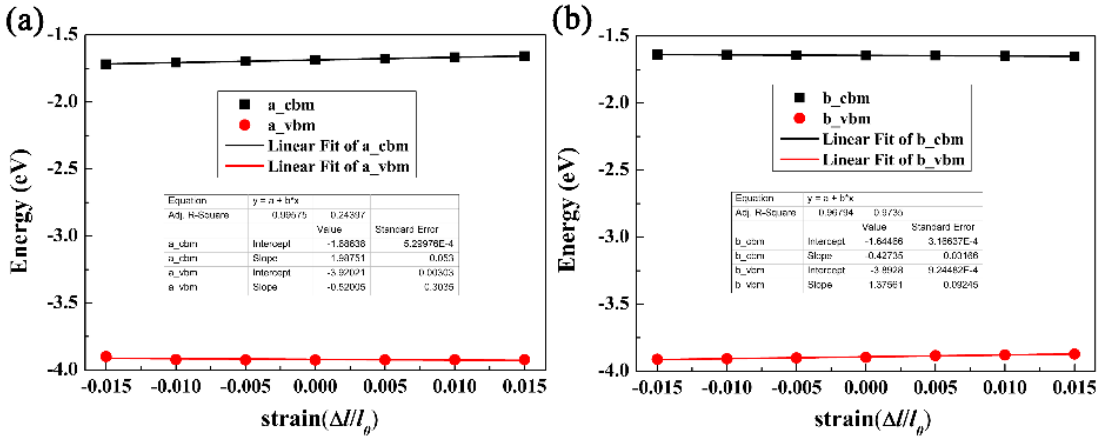

Figure S9. (a) The VBM/CBM shifts for monolayer KTlO with respect to the vacuum energy, as a function of the applied strain along the *a* direction. (b) The VBM/CBM shifts for monolayer KTlO with respect to the vacuum energy, as a function of the applied strain along the *b* direction. The linear fit of the data in (b) and (c) gives the deformation potential constants. All the calculations were based on the screened HSE06 hybrid functional.

Table S2. Calculated effective mass m^* (unit: m_e), deformation potential constant $|E_l^i|$ (unit: eV), elastic modulus C_{2D} (unit: N m^{-1}, both calculated with GGA-PBE), carrier mobility μ_{2D} (unit: 10^3 cm^2 V^{-1}s^{-1}) for monolayer KTlO along the *a* (*Y*-*M*) direction and *b* (*Y*-*Γ*) directions. The PBE and HSE06 results are included.

Method	Carrier type	m_a^*	m_b^*	$\|E_{la}\|$	$\|E_{lb}\|$	C_a^{2D}	C_b^{2D}	μ_a^{2D}	μ_b^{2D}
PBE	electron	0.740	1.120	2.00	0.46	25.97	26.26	0.20/**0.38**	2.54/**0.45**
	hole	2.407	2.434	0.23	1.54	25.97	26.26	1.86/**0.16**	0.04/**0.08**
HSE06	electron	0.474	0.624	1.99	0.43	25.97	26.26	0.54/**1.03**	9.04/**1.42**
	hole	1.582	1.468	0.52	1.38	25.97	26.26	0.85/**0.31**	0.13/**0.22**

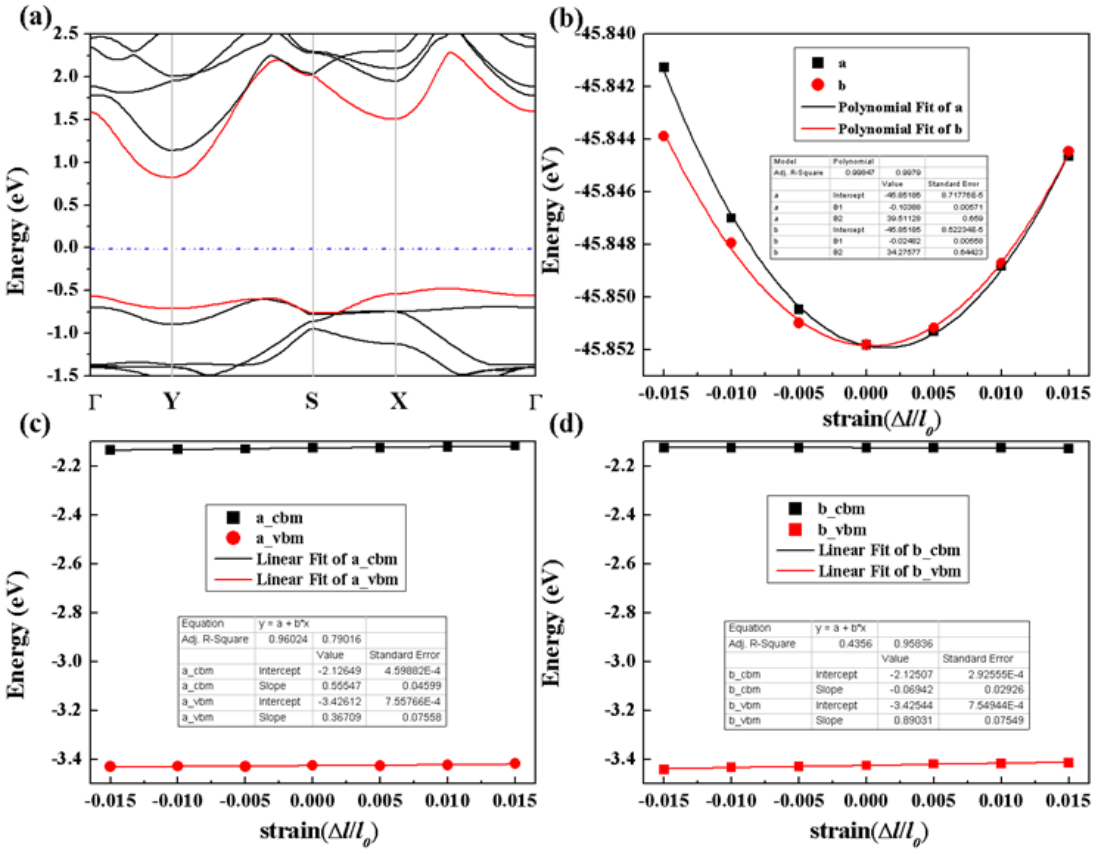

Figure S10. (a) The electronic band diagram of bilayer KTlO. (b) The relation between total energy and the applied strain δ along the *a* and *b* directions. The black and red fitting curves characterize the in-plane stiffness along the *a* and *b* directions of bilayer KTlO. (c) The shifts of VBM and CBM for bilayer KTlO with respect to the vacuum energy as a function of the applied uniaxial strain along the *a* direction. (d) The shifts of VBM and CBM for bilayer KTlO with respect to the vacuum energy as a function of the applied uniaxial strain along the *b* direction. The linear fits of the data in (c) and (d) yield the deformation potential constants. All the calculations were based on the PBE functional.

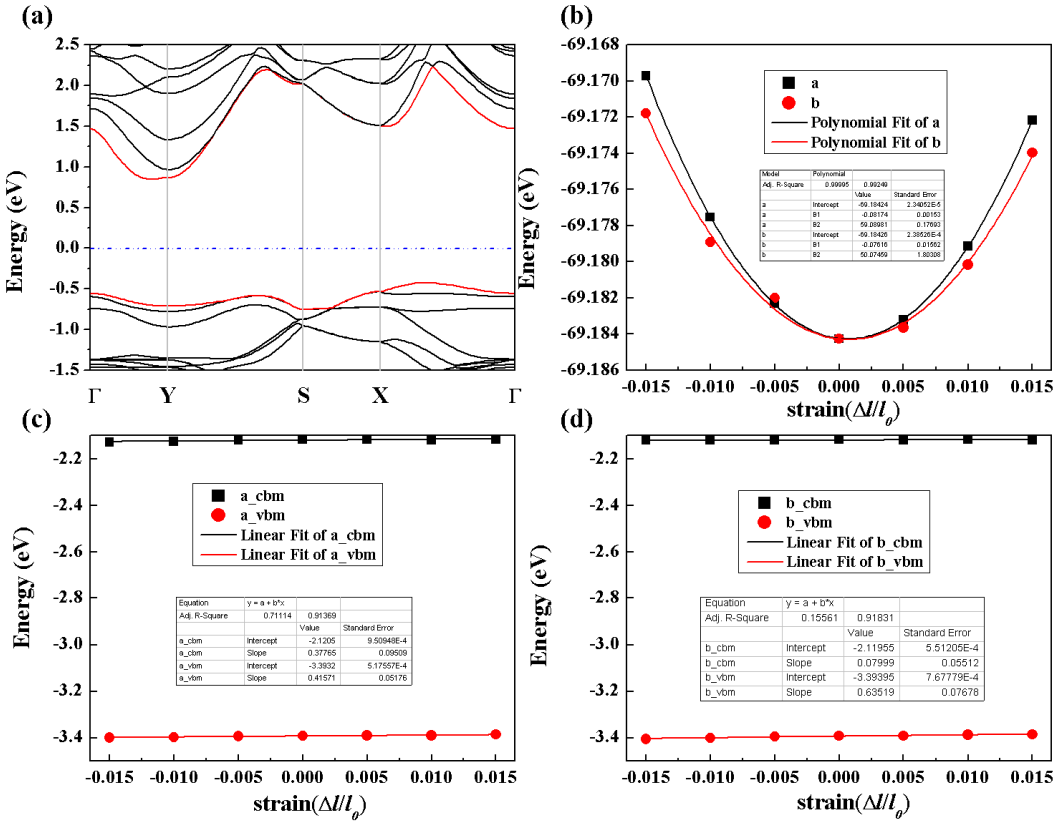

Figure S11. (a) The electronic band diagram of trilayer KTlO. (b) The relation between total energy and the applied strain δ along the *a* and *b* directions. The black and red fitting curves characterize the in-plane stiffness along the *a* and *b* directions of trilayer KTlO. (c) The shifts of VBM and CBM for trilayer KTlO with respect to the vacuum energy as a function of the applied uniaxial strain along the *a* direction. (d) The shifts of VBM and CBM for trilayer KTlO with respect to the vacuum energy as a function of the applied uniaxial strain along the *b* direction. The linear fits of the data in (c) and (d) yield the deformation potential constants. All the calculations were based on the PBE functional.

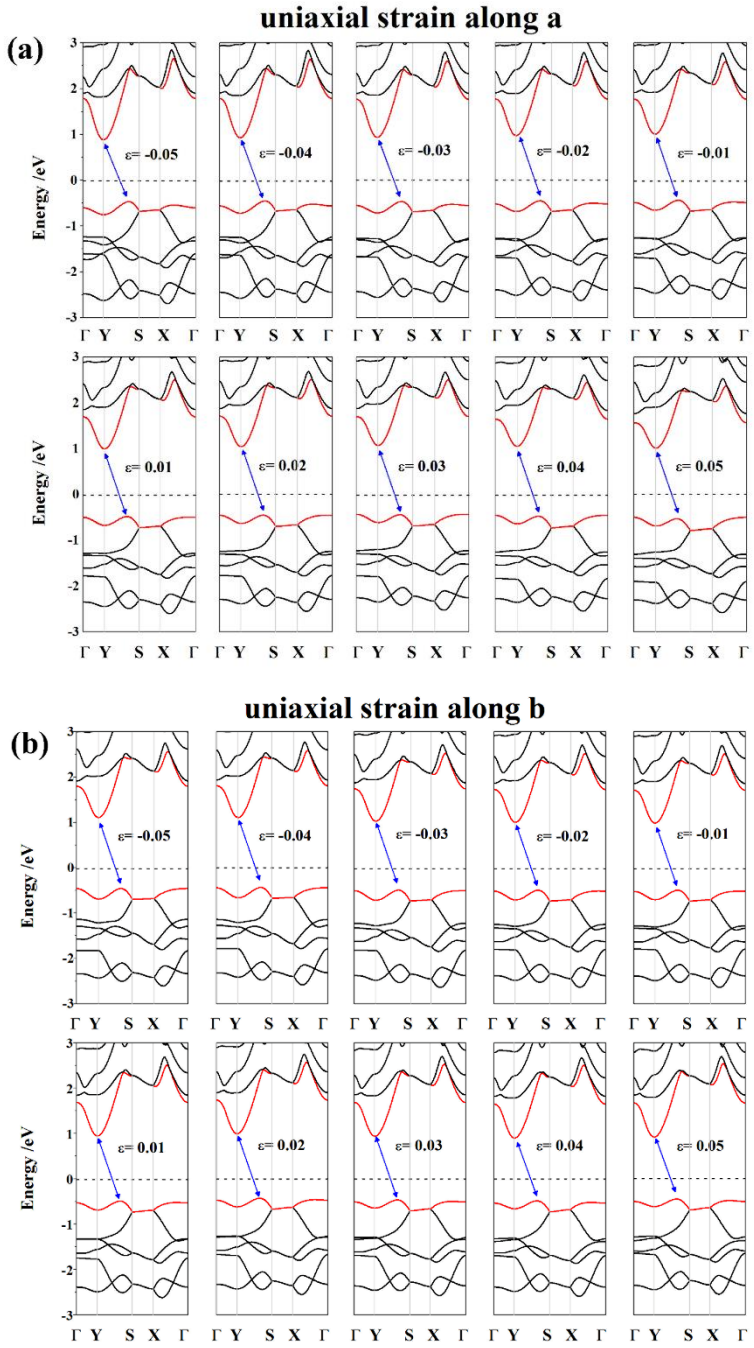
uniaxial strain along a
(a)
Energy /eV
ε= -0.05
ε= -0.04
ε= -0.03
ε= -0.02
ε= -0.01
ε= 0.01
ε= 0.02
ε= 0.03
ε= 0.04
ε= 0.05
Γ Y S X Γ
uniaxial strain along b
(b)
Energy /eV
ε= -0.05
ε= -0.04
ε= -0.03
ε= -0.02
ε= -0.01
ε= 0.01
ε= 0.02
ε= 0.03
ε= 0.04
ε= 0.05
Γ Y S X Γ

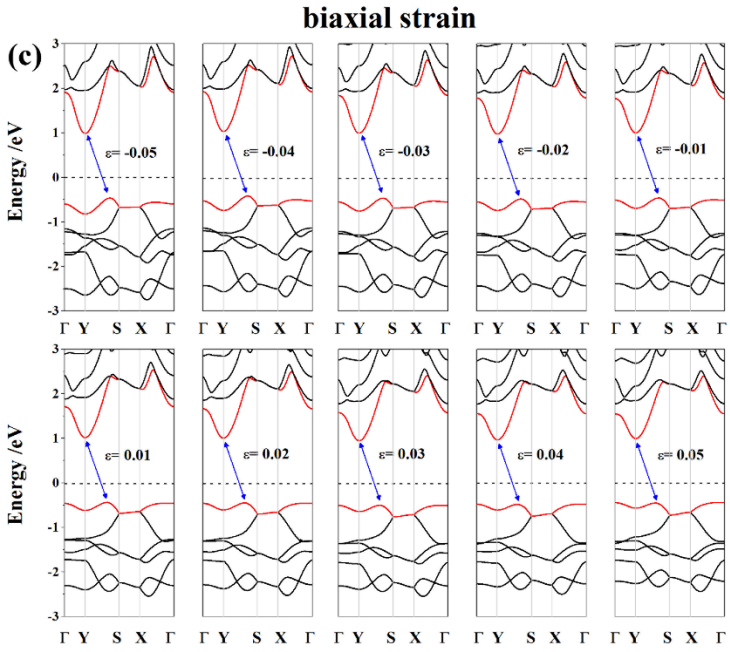

Figure S12. Electronic band structures of monolayer KTlO under various strain situations, calculated using the PBE functional. (a) Uniaxial strain along *a*-axis; (b) uniaxial strain along *b*-axis; (c) biaxial strain.

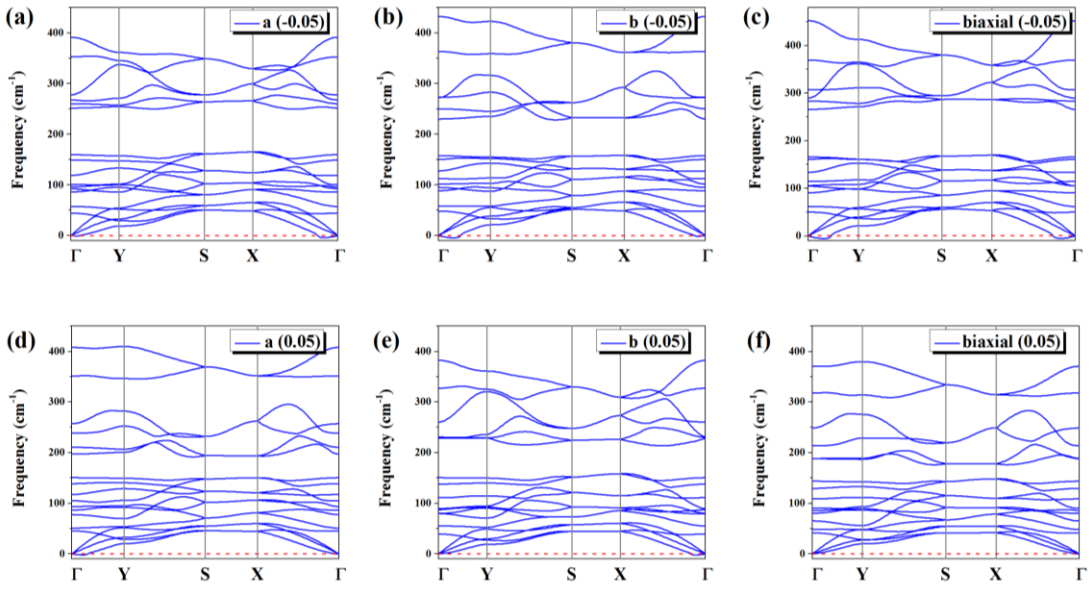

Figure S13. The calculated phonon dispersion spectra of monolayer KTlO under various strains. (a) Phonon dispersion of monolayer KTlO under -5% uniaxial strain along *a*-axis; (b) phonon dispersion of monolayer KTlO under -5% uniaxial strain along *b*-axis; (c) phonon dispersion of monolayer KTlO under -5% biaxial strain; (d) phonon dispersion of monolayer KTlO under 5% uniaxial strain along *a*-axis; (e) phonon dispersion of monolayer KTlO under 5% uniaxial strain along *b*-axis; (f) phonon dispersion of monolayer KTlO under 5% biaxial strain.

Table S3. Calculated elastic constants C_{ij} (N m^{-1}) of KTlO monolayer under various 5% strains (uniaxial and biaxial).

	Strain	C_{11}	C_{22}	C_{12}	C_{66}
a	-0.05	34.71	33.06	7.41	9.74
	0.05	22.60	25.34	5.75	11.56
b	-0.05	29.61	27.98	9.97	15.66
	0.05	27.46	26.82	4.86	8.12
biaxial	-0.05	38.43	35.49	12.81	14.93
	0.05	19.58	24.76	3.70	6.70

REFRENCES

(1) Ma, Y.; Kuc, A.; Heine, T. Single-Layer Tl_2O: A Metal-Shrouded 2D Semiconductor with High Electronic Mobility. *Journal of the American Chemical Society* **2017**, *139* (34), 11694–11697. https://doi.org/10.1021/jacs.7b06296.

(2) Hua, C.; Sheng, F.; Hu, Q.; Xu, Z.-A.; Lu, Y.; Zheng, Y. Dialkali-Metal Monochalcogenide Semiconductors with High Mobility and Tunable Magnetism. *J. Phys. Chem. Lett.* **2018**, 6695–6701. https://doi.org/10.1021/acs.jpclett.8b02859.